Original article

Phase-separated polyvinylidene fluoride/ZnO composite microspheres as sunlight-driven photocatalysts

Hayarunnisa Anwar [a], Maryam Al-Ejji [b,*], V. Radhika [c], Deepalekshmi Ponnamma [a,*]

[a] Materials Science and Technology Program, Department of Mathematics, Statistics and Physics, College of Arts and Sciences, Qatar University, 2713 Doha, Qatar
[b] Center for Advanced Materials, Qatar University, P O Box 2713, Doha, Qatar
[c] Department of Chemical Engineering, University of Calicut, Kerala, India

A B S T R A C T

PVDF-ZnO nanocomposites, prepared through phase separation-assisted nanoprecipitation with varying ZnO concentrations, exhibit enhanced photocatalytic performance against organic dye pollutants. Comprehensive characterization methods, including X-ray diffraction, spectroscopic and microscopic analyses, and thermal stability studies, are employed to assess the microspheres of phase-separated PVDF composites. Band gap analysis and optical characteristics of the nanocomposites are studied using Tauc's plots. The band gap energy of ZnO is determined as 3.47 eV, and the microsphere diameter averages between 0.23 and 0.24 μm. The incorporation of 1–3 wt% ZnO increases the decomposition temperature to approximately 480 °C. Photocatalytic performance tests utilizing various organic dye pollutants such as Methyl Orange (MO), Thymol Blue (TB), and Cresol Red (CR) reveal significant degradation efficiencies of 86 %, 84 %, and 35 %, respectively, under natural sunlight exposure. Despite the reduction in crystallinity of the phase-separated PVDF particles with the addition of ZnO, notable enhancements in the photocatalytic activity are achieved for the composites. Phase separation provides a synergistic interaction between the aligned polymer chains and the ZnO nanoparticles, contributing to the high degradation efficiency. Moreover, the presence of ZnO active photocatalytic sites induces active dye degradation. The study showcases the potentiality of PVDF/ZnO nanocomposites in photocatalytic dye degradation, with recoverability of composite particles from dye solutions, a simple composite development method, and direct exposure to natural sunlight. Significant implications are anticipated in pollution control and environmental remediation through the purification of industrial wastewater.

1. Introduction

Despite the industrial significance of dyes, their indiscriminate release into the environment during pre/post-production processes results in significant pollution. These wastes consist primarily of both organic and inorganic dyes, extensively used across diverse industries such as textiles (Gopal, 2019; Puzyn and Mostrag-Szlichtyng, 2012), paper and pulp (Mandeep et al., 2019; Ilyas et al., 2019), leather (Kanagaraj et al., 2015), paints (Fleischmann et al., 2015), cosmetics (Guerra et al., 2018), plastics (Patti and Acierno, 2022), and pharmaceuticals (Jain et al., 2005). Due to their complex chemical composition with a carbon basis, dyes inherently resist environmental degradation (Ong et al., 2018), making efficient removal or breakdown particularly challenging. It is imperative to eliminate these pollutants before discharging effluents into the environment, as they can pose serious health hazards, adversely affecting both human life and aquatic ecosystems. Many dyes are known to be carcinogenic (Gopal, 2019; Mandeep et al., 2019) and their high solubility in water makes complete elimination through conventional treatment processes challenging. In recent years, research efforts have focused on developing innovative technologies and materials for effectively removing and degrading dyes from industrial wastewater. However, classical treatment methods often exhibit poor effectiveness, high costs, or the generation of secondary pollutants (Bekru et al., 2022). Consequently, developing an environmentally friendly, efficient, and cost-effective dye degradation methodology becomes crucial (Ibrahim et al., 2016).

Photodegradation has emerged as a highly promising and extensively researched method for treating wastewater originating from industrial sources. This technique harnesses the power of photocatalytic materials to efficiently convert organic and inorganic contaminants into

less complex and non-toxic constituents (Hezam et al., 2022). Recently, scientists have directed their efforts towards advancing catalysts utilizing nanostructured materials as a potential substitute for current methodologies (He et al., 2023; He et al., 2022). Within this category, catalysts based on semiconductors, specifically zinc oxide (ZnO), have captured considerable interest, particularly in dye degradation (Parangusan et al., 2022). ZnO is an intriguing material that exhibits exceptional physicochemical properties when employed in photocatalytic applications (Parangusan et al., 2018). The unique combination of properties in ZnO, such as its high surface area, strong photocatalytic activity, and stability, make it an ideal candidate for efficient dye degradation in wastewater treatment. ZnO is a semiconductor with desirable attributes like high thermal conductivity, a large exciton binding energy (60 m eV), elevated electron mobility, and a wide band gap ranging from 3.2 to 3.4 eV (Zhang et al., 2009). To utilize the visible region of the solar energy spectrum in addition to the ultraviolet region, one approach is to form coupled semiconductors by incorporating narrow band gap semiconductors, given the wide band gap of the material (He et al., 2016). Many practices, such as developing heterostructures and combining with polymers, are employed for this purpose (He et al., 2021).

Poly (vinylidene fluoride) (PVDF) has emerged as a promising material for water treatment due to its inherent hydrophobicity, chemical resistance, biocompatibility, membrane-forming capabilities, and remarkable mechanical stability (Parangusan et al., 2022). These exceptional properties have made PVDF widely utilized in scientific research and various industrial processes (Kang and dong, Cao Y ming. , 2014). In line with this, our study aims to develop a photo-catalytically active material supported by a PVDF hydrophobic substrate, which facilitates the efficient recovery of the catalyst following photo-degradation. This approach reduces the risk of secondary pollution and allows for material reuse. By implementing this strategy, we aim to enhance the environmental sustainability and efficiency of catalyst separation processes. In literature, various fabrication methods have been reported for the synthesis of PVDF-ZnO composites, such as advanced electrospinning to create a ZnO-PVDF nanocomposite coating (Radwan et al., 2016). Kadir et al. developed tri-phase composite membranes consisting of an inorganic semiconductor, an organic polymer, and conducting nanofillers using the same nanocomposites (Kadir et al., 2020). While Pratihar et al. investigated the impact of ZnO nanorod's aspect ratio on the electrical properties of PVDF (Pratihar et al., 2020), Li et al. studied the pyroelectric properties of electrospun PVDF/ZnO composite fibers (Li et al., 2020). Regardless of the photocatalytic efficiency and dye degradation performance, all methods follow complicated processing steps and UV-assisted photocatalysis.

In this work, we successfully prepared a hydrophobic PVDF-ZnO composite by encapsulating photo-catalytically active nano ZnO in PVDF, using the phase separation-induced nanoprecipitation method (Mishra et al., 2022). Nanoprecipitation is a valuable technique for producing nanospheres and nanocapsules due to its simplicity, speed, and reproducibility (Rao and Geckeler, 2011). Phase separation provides distinct advantages in terms of efficiency, control over particle morphology, and thereby improved photocatalytic properties. We incorporated ZnO in different compositions into PVDF using two solvents of different polarities. The novelty of the work relies on the method of preparation of the ZnO/polymer composite by the phase separation method, which avoids the usual secondary pollution happening due to ZnO nanomaterials. The method allows enhanced surface availability to significantly improve the rate of photocatalysis when compared to the composite thin films of fibers. Composite particles were produced by incorporating various compositions of ZnO, such as 1 wt%, 2 wt%, and 3 wt%. All resulting samples were comprehensively characterized using XRD, FT-IR, TGA, and DSC analysis techniques. Furthermore, the photocatalytic degradation efficiency of composites was studied using three different dyes, Cresol Red (CR), Methyl Orange (MO), and Thymol Blue (TB). The primary objective of

this study is to elucidate the prospective utility of these artificially produced materials within the realm of photocatalysis.

2. Experimental techniques

2.1. Materials

Zinc Acetate dihydrate $(Zn(CH_3COO)_2 \cdot 2H_2O)$ and sodium hydroxide (NaOH) were used as precursor chemicals for nano ZnO. PVDF, Acetone (CH_3COCH_3), methanol (CH_3OH) and the dyes MO, TB, and CR were purchased from Sigma -Aldrich and used without further purification. Purified water used for the analysis was obtained from the Millipore Milli-Q water system.

2.2. Synthesis of ZnO nanoparticles

Nano ZnO was prepared using the co-precipitation method. To prepare the precursor solutions, 1 M NaOH and 0.5 M $Zn(CH_3COO)_2 \cdot 2H_2O$ solutions were separately prepared in deionized water. These solutions were then mixed dropwise with magnetic stirring, and kept under constant stirring for about 2 h at room temperature. The resulting precipitate was separated by centrifugation, washed with deionized water and acetone until neutral, and dried in an oven at 75 °C for approximately 1.5 h. The dried sample was powdered using an agitar mortar and weighed.

2.3. Synthesis of phase-separated PVDF-ZnO composite microspheres

PVDF microspheres were prepared using a phase separation-induced nanoprecipitation method with a solvent-antisolvent procedure, as illustrated in Fig. 1. PVDF (0.1 g) was dispersed in 20 ml acetone (solvent) by handshaking in a centrifuge tube. A mixture of methanol–water (1:1) [anti solvent] was injected slowly from the bottom end of the centrifuge tube with the PVDF dispersion. PVDF microspheres were precipitated at the solvent-anti-solvent interface and deposited at the bottom end of the centrifuge tube. The precipitate was separated by centrifugation, washed with ethanol at 4000 rpm, and dried in an oven at 80 °C for 6 h.

PVDF-ZnO composite particles were synthesized by adding various percentages (1 wt%, 2 wt%, 3 wt%,) of ZnO to the precursor PVDF-Acetone dispersion. This was achieved by sonicating specific amounts of ZnO, (0.001, 0.002 and 0.003 g for respective 1 wt%, 2 wt%, 3 wt% compositions) in 5 ml acetone for 1 h, followed by mixing it with the PVDF dispersion in acetone to make the total solvent amount 20 ml. The solution was magnetically stirred overnight at 1500 rpm to achieve homogeneous dispersion of ZnO in PVDF. Phase separation was induced after overnight stirring, followed by centrifugation and washing procedures as done for neat PVDF.

2.4. Characterization techniques

The crystalline structure of the samples was determined using an X-Ray diffractometer (EMPYREAN, PANalytical Co., Almelo, Netherlands) operating with CuKα radiation ($\lambda = 0.1564$ nm) in the 2θ range of 10° to 80°, at 45 kV and 40 mA. Fourier-transform infrared spectroscopy (FTIR) analysis was conducted in transmission mode using a PerkinElmer Spectrum 400 spectroscope in the wavelength range of 400 to 4000 cm^{-1}, with a resolution of 2 cm^{-1}. UV–visible spectroscopic experiments were carried out using a Biochrom UV–Visible spectrophotometer, scanning samples within the wavelength range of 200–900 nm. The morphological characteristic of ZnO was investigated using a transmission electron microscope (TEM; FEI TEM, Model Tecnai G2 S Twin F20), and the microspheres morphology was studied using a scanning electron microscope (SEM; Nova Nano SEM 450) equipped with an EDAX. The crystallinity of the samples was determined using a Perkin Elmer DSC 4000 differential scanning calorimeter (DSC) by
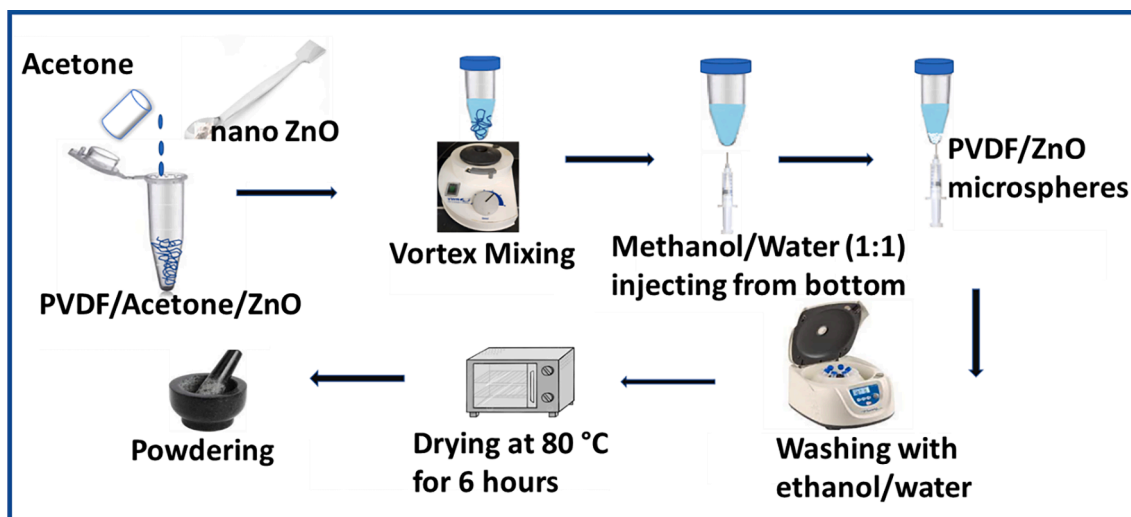
Fig. 1. Schematic diagram of preparation of PVDF-ZnO composite.

heating samples between 30 and 350 °C at 10 °C/min^{-1} under a nitrogen atmosphere. Thermogravimetric analysis (TGA) was performed using a Perkin Elmer TGA 4000 at a heating rate of 10 °C/min^{-1} from 30 to 800 °C under a nitrogen atmosphere. Photocatalytic experiments were conducted in sunlight using solutions of MO, TB and CR dyes with concentrations of 10 ppm. For each dye, 5 ml of solution was used, and
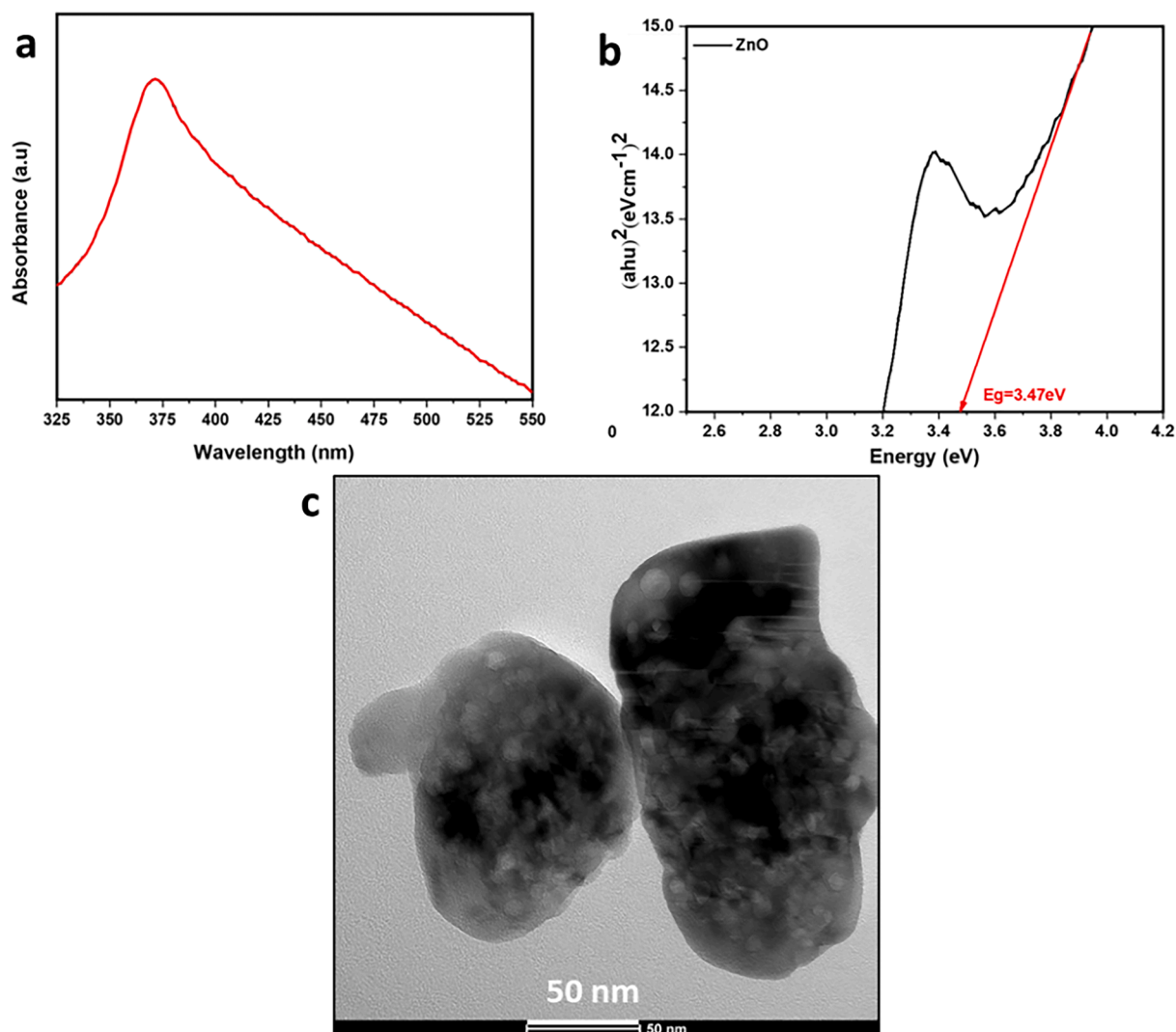

Fig. 2. (a) UV –visible spectrum and (b) Tauc plot for the ZnO nanoparticles (c) TEM image for ZnO.

0.02 g of the prepared nanocomposite was added to test degradation efficiency. The absorbance of the solutions before and after sunlight exposure was measured at intervals of 0.5 h, 1 h, 2 h, 3 h, and 6 h using a UV–visible spectrophotometer.

3. Results and discussion

3.1. Structural, morphological and electronic properties of ZnO

The structural characterization of the ZnO nanoparticles was conducted through FTIR and XRD analyses, as depicted in Fig. S1 (Supporting Information). In the FTIR spectrum (Fig. S1a), a prominent peak at approximately 3359.78 cm^{-1} corresponds to the characteristic vibrational mode of –OH bonds. Peaks identified at 1650, 1400 and 1054 cm^{-1} are associated with Zn-O vibrational bands in the ZnO nanoparticles (Mallakpour and Madani, 2012; Zhao and Shen, 2012; Ling et al., 2013), while the peak at 890 cm^{-1} corresponds to the vibrational mode associated with Zn-O bonds. Additionally, the peak at 1504 cm^{-1} is attributed to unreacted zinc acetate precursor in ZnO. The spectrum displays a relatively smooth profile, indicating a lack of significant vibrational modes or bonding interactions involving other elements, highlighting the predominance of zinc (Zn) and oxygen (O) in the nanoparticles' composition. The absence of significant peaks originating from other elements further reinforces the purity of the ZnONPs under investigation, with only minimal traces of CO_2 detected (Handore et al., 2014).

Fig. S1b illustrates the X-ray diffraction pattern of the ZnO nanopowder, with peaks detected at approximately 31°, 35°, 36°, 48°, 57°, 63°, 68°, 69°, and 75° corresponding to the (100), (102), (101), (102), (110), (103), (112), (201), and (004) crystallographic planes, respectively, associated with the hexagonal wurtzite phase of ZnO (Zhou et al., 2007; Khoshhesab et al., 2011). No additional XRD peaks were observed, indicating the absence of impurities in the synthesized ZnONPs (Talam et al., 2012).

In Fig. 2a, the UV–Visible absorbance spectrum for ZnO nanoparticles dispersed in water reveals an absorption peak at approximately 375 nm, corresponding to the hexagonal wurtzite structure of ZnO (Wooten et al., 2009). This observation represents a red shift compared to bulk ZnO (365 nm) by approximately 10 nm (Suwanboon and Amornpitoksuk, 2012), which can be attributed to shallow levels within the band gap, often due to foreign atoms in the lattice (Reddy et al., 2011). The redshift indicates a reduction in the optical band gap, particularly concerning the energy of the first bright exciton (Baskoutas and Bester, 2010; Baskoutas and Bester, 2011), attributed to quantum confinement and crystal defects (Reddy et al., 2011). The band gap of a semiconductor refers to the energy separation between its valence band and conduction band, where no energy levels are available. This parameter is crucial, as it dictates the minimum energy of photons required to generate photoelectrons and holes within the semiconductor. Tauc's equation (Equation (1) was utilized on the UV–visible absorbance data to determine the band gaps (Fig. 2b).

For materials with a direct band gap (Baskoutas and Bester, 2011), the equation is expressed as follows:

$$(\alpha h\upsilon)^2 = k\left(h\upsilon - E_g\right) \tag{1}$$

where $h\nu$ is the photon energy, E_g is the band gap energy, k is a constant, and α is the absorption constant.

Equation (1) can be further expressed as:

$$(2.303^* A^* 1240/\lambda)^2 = k\left(1240/\lambda - Eg\right) \tag{2}$$

where A and λ are absorbance and wavelength, respectively, obtained from the absorption spectra of ZnO. This equation is used to plot the absorption curve (Fig. 2b), and the tangent of the curve was used to determine the energy band gap of the nanoparticles (Ekennia et al.,

2021). Previous investigations have documented band gap energies of biosynthesized ZnO nanoparticles as 2.88 eV and 3.10 eV (Gonçalves et al., 2021), as well as 3.28 eV (Suresh et al., 2018), 3.31 eV (Al-Ariki et al., 2021), and 3.51 eV (Akhtar et al., 2015). In our case, the band gap energy of ZnO was determined to be 3.47 eV, which falls within the reported range. The particle morphology was also examined using transmission electron microscopy (TEM). Fig. 2c displays the TEM image of the synthesized ZnO nanomaterials, revealing particle dimensions ranging between 50 nm and 100 nm.

3.2. Structural, morphological and thermal properties of phase-separated PVDF/ZnO microspheres

The structural characteristics of pure PVDF and PVDF-ZnO composite microspheres were assessed using XRD patterns, as given in Fig. 3. A small but distinct peak is observed at a 20° diffraction angle for all samples, corresponding to the polymer chains. Previous studies indicate that this peak corresponds to the (200) plane of the PVDF β-phase, indicating the semicrystalline nature of PVDF (Devi and Ramachandran, 2011; Singh et al., 2006; Rajendran et al., 2007). The peak consistently remained at the same position for all composites, indicating the uniform dispersion of ZnO within the polymer. As the ZnO concentration increases, the intensity of peaks enhances, attributed to the improved interaction of PVDF chains with ZnO, consequently influencing the degree of crystallinity (Ma et al., 2002). The crystallinity values were calculated for all composites, showing a trend from 34.23 to 37.60 % from PVDF to PVDF-ZnO at 3 wt%., as expected. Additionally, all composites exhibit minor peaks corresponding to the ZnO crystalline planes (typically around 30–40° diffraction angles), with peaks around 31.8°, 34.4°, and 36.3° (2θ values) corresponding to the (100), (002), and (101) crystal planes of ZnO; however, these peaks have diminished intensity as the concentration of ZnO is comparatively lesser. It is worth mentioning that the structural stability and crystallinity promote charge separation and transfer, influencing the photocatalytic activities of the composites. Higher crystallinity leads to improved charge carrier mobility and longer carrier lifetime, and the orientation causes better interaction of photons with target pollutants during photocatalysis. Fig. 3b presents the FTIR spectra for the PVDF and composite microspheres, further elucidating the physical interaction of ZnO with PVDF without the formation of any additional chemical bonding. All vibration bands correspond to different stretching and bending vibrations of the PVDF molecular chains. Specifically, the peaks at 1179 cm^{-1} and 1397 cm^{-1} in all composites relate to C-F bond vibrations in the PVDF skeleton. When compared with neat PVDF, there is a slight change in the intensity of these peaks in the ZnO-containing composite microspheres, which can be attributed to the influence of Zn-O bonding vibrations on the PVDF skeleton. However, the comparatively lesser amount of ZnO is the reason behind the less significant variation in this case.

The morphological analysis of the phase-separated particles was conducted using SEM images, as depicted in Fig. 4. During phase separation at the interface, the microspheres begin to form and settle at the bottom of the tube through diffusion-assisted precipitation (Mishra et al., 2022). As indicated in a previous study (Mishra et al., 2022), the interactions between the –CF$_2$ dipoles of the PVDF chains and water molecules lead to the self-folding of the polymer, resulting in the formation of microspheres, which consistently occur at the solvent interface. Introducing the non-polar solvent, acetone, to the medium interrupts the hydrogen bonds between water molecules, creating voids. Simultaneously, this process can initiate new hydrogen bond formations between neighbouring water molecules, preventing longer polymeric chains from entering the voids. This reduces the surface area and subsequently affects the formation of polymer microspheres. The SEM image clearly shows the spherical morphology of all particles, and the average particle size distribution indicates no significant influence on particle size with varying ZnO concentration. The ZnO particles formed a nanoflake structure, as depicted in the inset of Fig. 4b; however, these
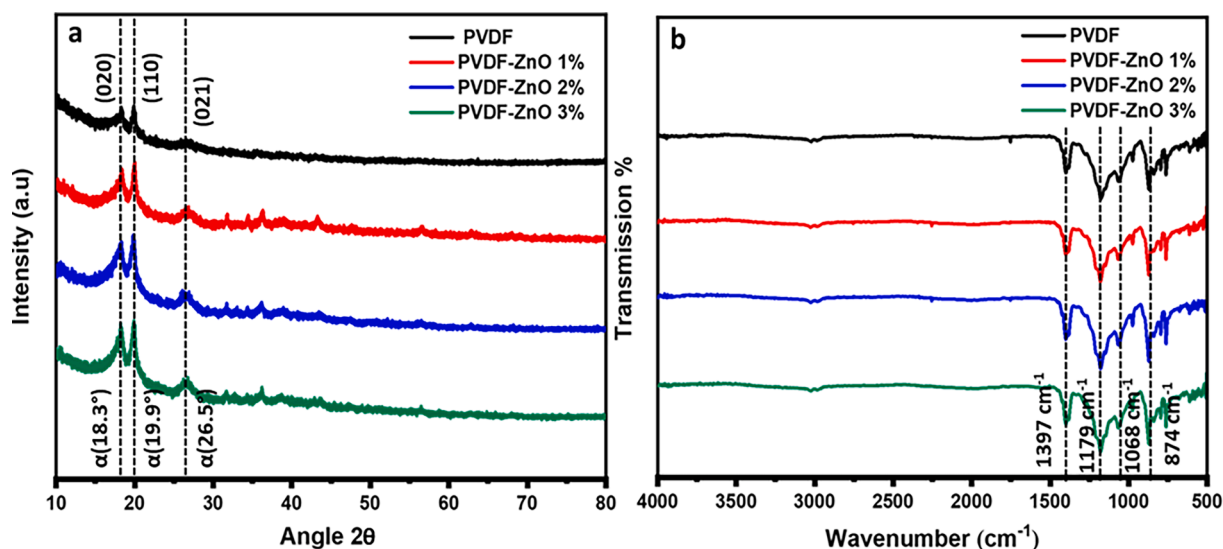
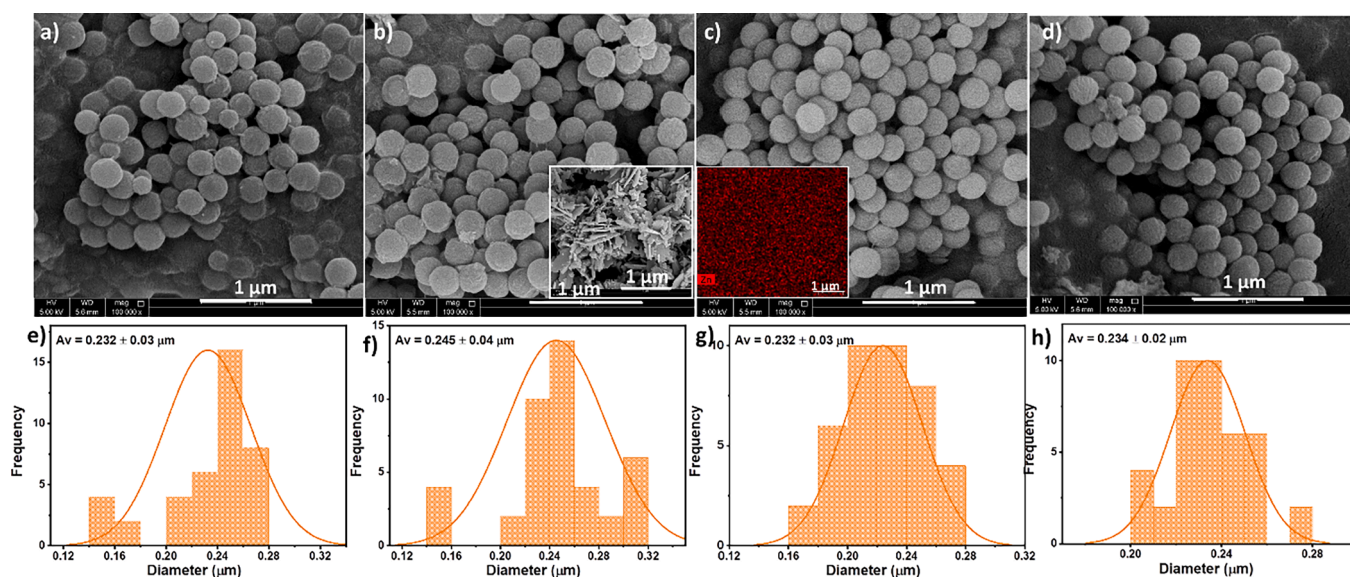**Fig. 3.** (a) XRD and (b) FTIR for PVDF-ZnO nanocomposite.

Fig. 4. Morphology analysis of PVDF and PVDF/ZnO composite particles, with corresponding size distribution curves; a) and e) PVDF; b) and f) PVDF-ZnO (1 wt%); c) and g) PVDF-ZnO (2 wt%); d) and h) PVDF-ZnO (3 wt%). Inset of b) SEM image of ZnO, and c) EDX mapping image of the microsphere with Zn distribution.

structures are consistently enveloped within the polymer chains in the nanocomposite morphologies. This uniform and well-distributed arrangement of microspheres within the polymer medium (also evidenced from the EDX mapping image in the Fig. 4c inset) during composite preparation can be attributed to this phenomenon.

The endothermal and exothermal curves obtained from the differential scanning calorimetry (DSC) analysis of PVDF and its nanocomposites were examined (Fig. S2). A comparison between PVDF-ZnO and the pure polymer revealed a slight improvement in crystallization and melting temperatures. However, minimal variations were observed when different concentrations of ZnO (1 wt%, 2 wt%, and 3 wt%) were compared. The presence of ZnO in the nanocomposite acted as a nucleating agent, accounting for the observed effects on crystallization and melting temperatures (Yang et al., 2014). Interestingly, slight increases were observed in the melting and crystallization temperatures when comparing the PVDF-ZnO nanocomposite to pure PVDF. These findings suggest that incorporating ZnO into the PVDF matrix influences its crystallization behaviour, primarily by affecting the polymer chain

mobility and kinetics. The results indicate the potential of PVDF-ZnO nanocomposites in improving structural stability and promoting strong intermolecular forces.
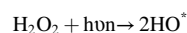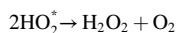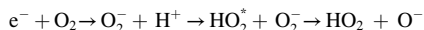
The thermogravimetric and derivative thermogravimetric curves were obtained for the PVDF-ZnO nanocomposite particles, as shown in Fig. S3. The curves indicate that the PVDF composites exhibit excellent stability up to approximately 480 °C, beyond which degradation occurs. In comparison, the pure PVDF material shows a decomposition temperature of around 450 °C. However, with the addition of ZnO (Du et al., 2018), the decomposition temperature increases to approximately 480 °C. This enhancement can be attributed to the effective dispersion of ZnO within the PVDF polymer matrix, which restricts the mobility of PVDF chains. The presence of well-dispersed nanoparticles leads to a higher crosslink density, stronger adhesion with the polymer chains, and improved crystallinity, consequently improving thermal stability (Tsai et al., 2011). Moreover, the PVDF-ZnO nanocomposite exhibits a remarkable improvement in thermal stability, achieving temperatures as high as 480 °C when incorporating 1–3 wt% of ZnO.

3.3. Photocatalytic activity of PVDF-ZnO composite microspheres

In the photocatalytic decomposition of dye pollutants, the excitation of electrons creates electron-hole pairs between the conduction and valence bands. The photogenerated holes (h^+) in the valence band subsequently react with either water molecules or hydroxide ions (OH^-). The following reaction can describe this phenomenon.

$$h^+ + H_2O \rightarrow OH^* + H^+$$

$$h^+ + OH^- \rightarrow OH^*$$
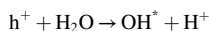
Meanwhile, the electrons (e^-) in the conduction band react with the O_2 and generate O_2, forming OH* radicals. The generated species finally decompose the dye molecules.

$$e^- + O_2 \rightarrow O_2^- + H^+ \rightarrow HO_2^* + O_2^- \rightarrow HO_2 + O^-$$

$$2HO_2^* \rightarrow H_2O_2 + O_2$$

$$H_2O_2 + h\upsilon n \rightarrow 2HO^*$$

$$HO^* + O^- + Pollutant \rightarrow CO_2 + H_2O$$

In the PVDF-ZnO microspheres, the photocatalytic mechanism (Fig. 5) begins with the absorption of photons by uniformly distributed ZnO, leading to the generation of electron-hole pairs in its conduction and valence bands, respectively. These electron-hole pairs migrate to the surface of the ZnO particles, where they participate in redox reactions with adsorbed species, such as water molecules or hydroxide ions (OH—), as explained before. Specifically, photogenerated holes (h^+) in the valence band can oxidize water molecules or hydroxide ions to produce hydroxyl radicals (OH•), which are highly reactive and contribute to the degradation of organic pollutants. Meanwhile, photogenerated electrons (e-) in the conduction band can reduce oxygen molecules to form superoxide radicals (O_2•-), which also participate in oxidative reactions with organic molecules. Additionally, the presence of the polymer composite microsphere provides a stable support matrix for the ZnO nanoparticles, ensuring their uniform distribution and facilitating the adsorption of dye molecules onto the catalyst surface. This enhanced adsorption, combined with the efficient charge separation and transfer properties of ZnO, promotes the degradation of various dye molecules through oxidative and/or reductive pathways, ultimately leading to the effective removal of pollutants from the environment.

The photocatalytic properties of all PVDF/ZnO composite particles were thoroughly examined using three organic dyes, namely MO, TB, and CR. The PVDF-ZnO composite fabricated through the phase separation assisted nanoprecipitation technique facilitates high surface area and exposure of ZnO active sites within the composites. This interaction between the dye molecules and ZnO active sites enhances photon absorption, generating electron-hole pairs that initiate the photocatalytic process. For the photocatalytic experiments, solutions of the three dyes were prepared at a concentration of 10 ppm. Subsequently, 5 ml of each dye solution was measured, and 0.02 g of the PVDF-ZnO nanocomposite was added to each solution. The absorbance of the dyes was measured at specific intervals (0.5, 1, 2, 3, and 6 h) using a spectrophotometer. Though PVDF is a favourable choice for fabricating mechanically and chemically stable nanocomposites through the phase separation method, the polymer does not possess any inherent photocatalytic properties (Kang and dong, Cao Y ming. , 2014). Using the nano-precipitation technique, synthesizing the PVDF-ZnO composite at various ZnO concentrations (1 wt%, 2 wt%, and 3 wt%) ensured the successful incorporation of ZnO active sites onto PVDF chains. By monitoring the absorbance of the dyes at various time intervals, we could quantitatively evaluate the photocatalytic activity of the composites. The results obtained from this comprehensive investigation provide valuable insights into the photocatalytic efficiency of the PVDF-ZnO composite, thereby elucidating its potential applications in environmental remediation and wastewater treatment. Moreover, the findings offer valuable information on the impact of ZnO concentration on the photocatalytic behaviour of the composite material.

To investigate the degradation process and reusability of PVDF-ZnO composites towards different concentrations of CR dye (1 %, 2 %, and 3 %), absorption spectra and cyclic photodegradation experiments were conducted, as depicted in Fig. 6a, b, and c. Continuous monitoring of the UV absorption spectra of CR observes noticeable changes in absorbance under prolonged light exposure. The results demonstrate a decreasing trend in absorbance as the irradiation time increases. In particular, a significant weakening of the absorption peak intensity was observed after 6 h of irradiation, indicating a substantial decrease in CR concentration within the solution. The degradation efficiencies are quantified by comparing the absorbance values obtained from the UV–visible spectral analysis. The degradation typically results in a decrease in absorbance values with respect to the time of reaction, concentration of ZnO, available surface interactions of catalysts with pollutants, etc. These findings provide in-depth analysis of the remarkable photocatalytic activity of the PVDF-ZnO composites.

Additionally, the impact of varying ZnO concentrations within the PVDF-ZnO nanocomposites on the photodegradation of CR is compared using the photodegradation rate versus the time plots (Fig. 6d). At higher ZnO concentrations (2 and 3 wt%), there may be an increased
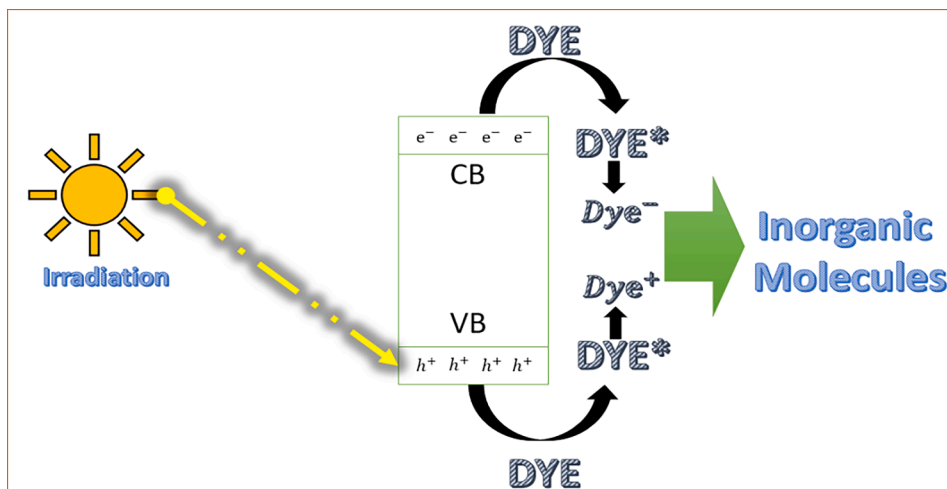

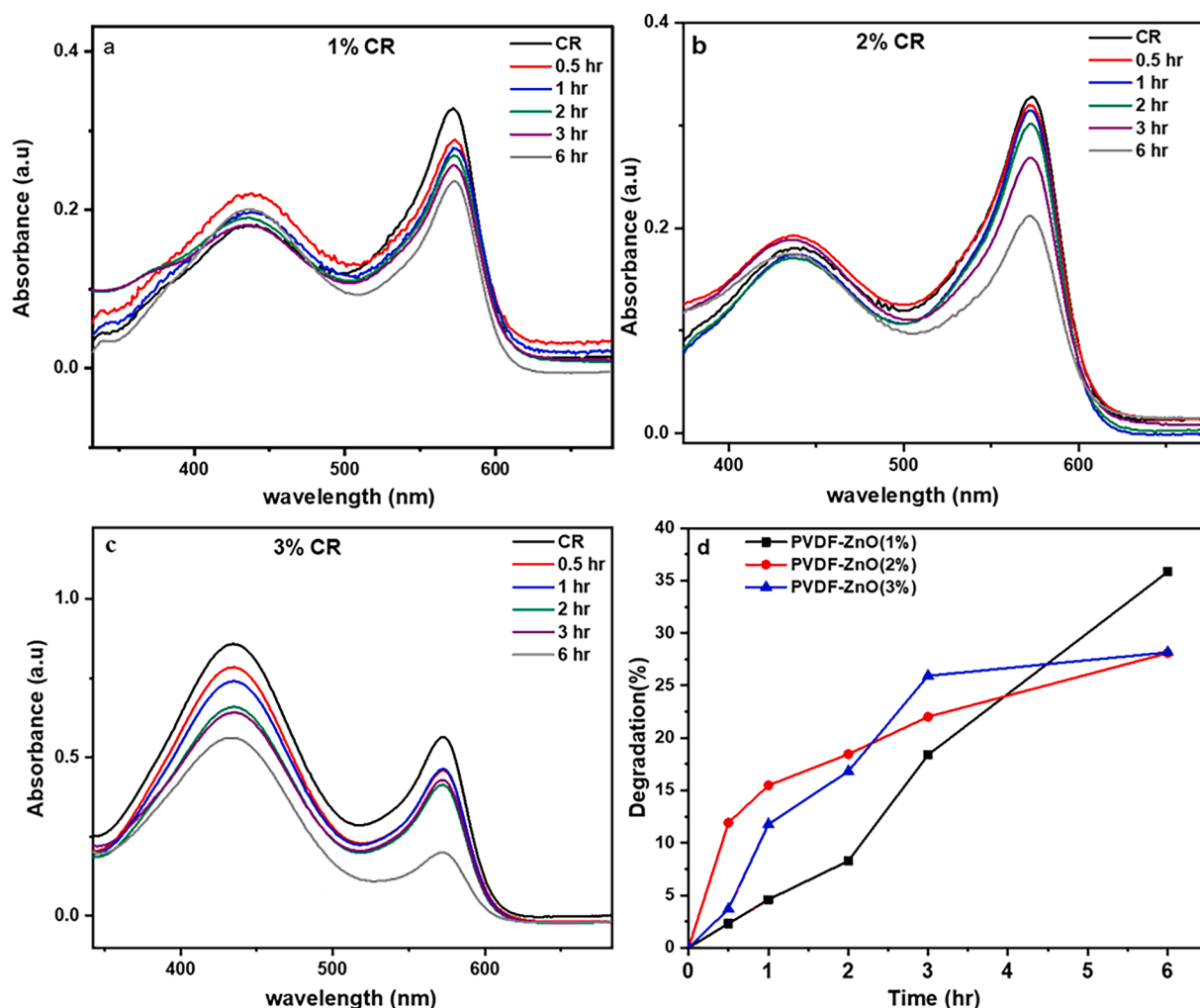**Fig. 5.** Mechanism of photocatalysis of dye pollutants.

Fig. 6. The degradation of CR by PVDF-ZnO nanocomposites with different ZnO compositions a) 1 wt%, (b) 2 wt%, (c) 3 wt% and (d) comparison of degradation efficiency.

number of active sites for photocatalytic reactions, leading to initially higher degradation rates. However, as the reaction progresses, agglomeration of ZnO particles or excessive surface coverage may occur, reducing the effective surface area and catalytic activity over time. On the other hand, at lower ZnO concentration (1 wt%), while the initial active sites may be fewer, the dispersion of ZnO particles may be more uniform, allowing for sustained catalytic activity over the longer term. After 6 h of photocatalysis, the highest degradation percentage is achieved for a ZnO concentration of 1 wt%, reaching 35 %.

Fig. 7 exhibits the absorption spectra and degradation kinetics of the PVDF-ZnO composite microspheres using the MO dye. The results consistently show a decrease in absorbance as the duration of the irradiation increases, with a notable weakening of the absorption peak observed after 6 h of exposure. This indicates a substantial reduction in the concentration of MO within the solution, highlighting the remarkable photocatalytic activity of the PVDF-ZnO composites. This study emphasizes the composites' potential for effectively degrading MO dye, highlighting the applications of PVDF-ZnO composites in photocatalysis and wastewater treatment. In addition, the variation in photodegradation over time, as depicted in Fig. 7d, clearly illustrates a decline in photodegradation efficiency with increased concentrations of ZnO from 1 wt% to 3 wt%. Interestingly, the PVDF-ZnO 1 wt% nanocomposite exhibited the highest level of photodegradation (the reasons were explained earlier), reaching an impressive rate of 86 % in this study. Additionally, we explored the reusability of these composites,

revealing their promise as sustainable and cost-effective solutions.

Similarly, the photocatalytic efficiency of the microspheres was tested using different dye compositions of TB (Fig. 8). The UV absorption spectra of TB were continuously monitored throughout prolonged light irradiation to observe any variations in absorbance. The results demonstrate a consistent decrease in absorbance as the irradiation time progresses. After 6 h of irradiation, a significant weakening of the absorption peak was observed, indicating a substantial reduction in TB concentration. These findings also strongly emphasize the exceptional photocatalytic activity exhibited by the PVDF-ZnO composites. As represented in Fig. 8d, a decrease in the efficiency of photodegradation was observed with increasing ZnO concentration from 1 to 3 wt%. It is important to highlight that among all the samples studied, the PVDF-ZnO nanocomposite with a 1 wt% ZnO concentration displayed the highest rate of photodegradation, reaching 84 %. These findings suggest the existence of an optimal ZnO concentration for achieving efficient photodegradation of all dye solutions. The primary reason for this activity is the microsphere's morphology, as smaller particles possess a larger number of active surface sites, which can enhance photocatalytic performance (Dodd et al., 2006; He et al., 2022).

Furthermore, the investigation also explored the reusability of composites, underscoring their potential as sustainable and cost-effective solutions. After photocatalysis, the solutions were centrifuged to remove all particles, and the total organic content (TOC) values were detected. The values were comparable to those of normal distilled water,
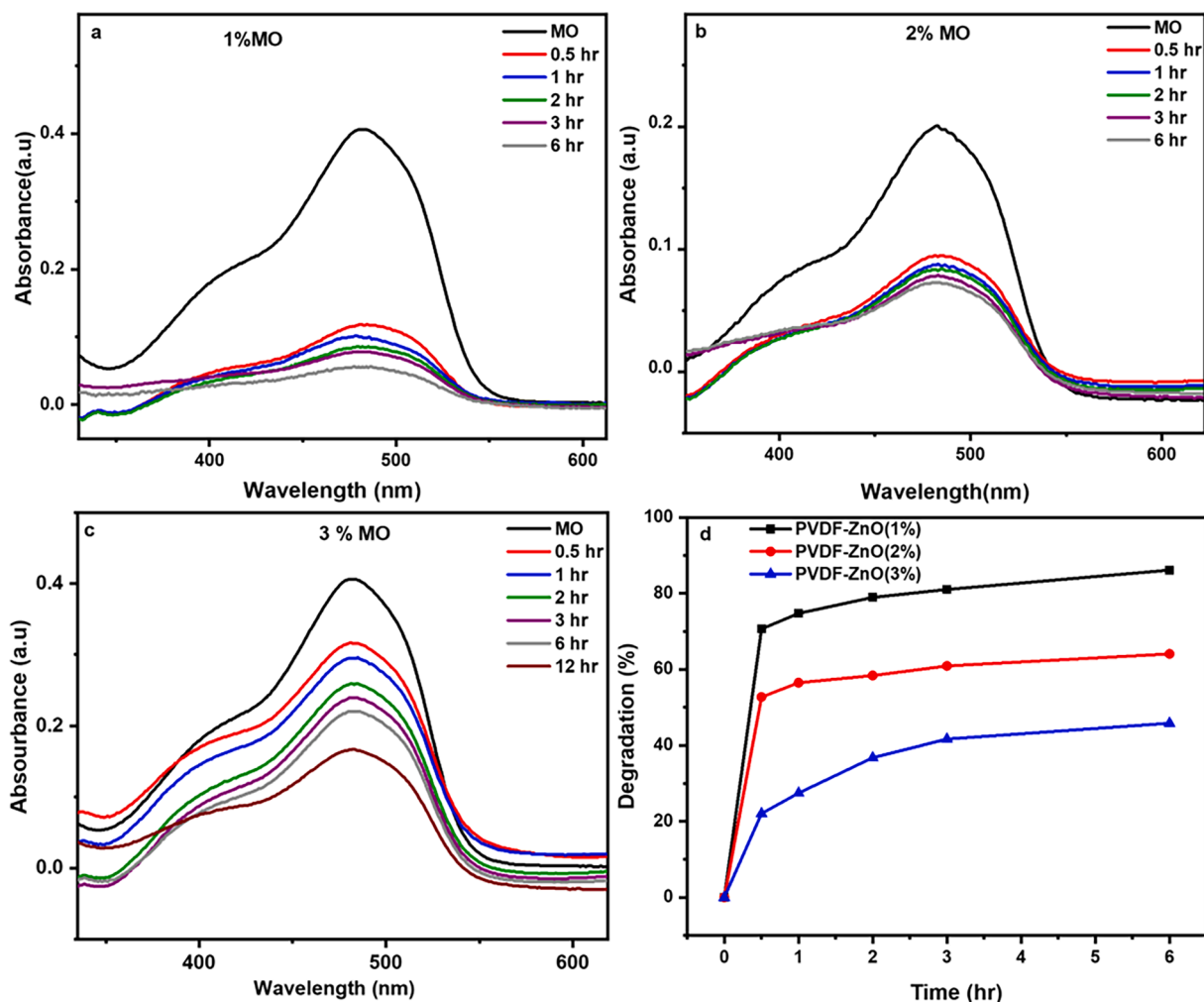
Fig. 7. The degradation of MO by PVDF-ZnO nanocomposites with different ZnO compositions a) 1 wt%, (b) 2 wt%, (c) 3 wt% and (d) comparison of degradation efficiency.

confirming the absence of leaching or secondary pollution.

In all the photocatalytic degradation studies, the composite with 1 wt % ZnO demonstrates the highest efficiency rate, influenced by several experimental factors. The primary influence of this composition lies in the uniform distribution of particles within the PVDF, enhancing chemistry and reactivity compared to other ZnO compositions. This uniform distribution also affects charge carrier dynamics, facilitating the migration of photogenerated electron-hole pairs. As the 1 wt% ZnO achieves ideal uniformity, it influences band gap dynamics, thereby improving photocatalytic dye degradation.

Photocatalytic dye degradation in the presence of ZnO-reinforced materials can be well described using mathematical modelling. The reaction follows pseudo-first-order kinetics, as demonstrated in Fig. 9. The corresponding mathematical equation can be defined as the following.

$$Degradation \ (\%) = \left(\frac{C_0 - C_t}{C_0}\right)100 \qquad (3)$$

C_0 and C_t represent the initial and final concentration of the dye solution, respectively, before and after the radiation exposure. In the dye-degradation process, the concentration of the nanocatalyst generally exceeds that of the dye molecules in the medium, ensuring a relatively constant dye composition conducive to pseudo-first-order kinetics. Fig. 9 shows the pseudo-first-order reaction kinetics for all compositions of ZnO nanoparticles in CR, MO and TB dye degradation. The wide band gap, high electron mobility and ZnO photostability typically facilitate

the formation of photogenerated electron-hole pairs for effective charge transfer. Despite the polymer chains covering the active ZnO sites in the composite preparation, the surface area and porosity of the prepared PVDF-ZnO microspheres remain highly beneficial due to the phase separation mechanism. Upon contact with the active sites of ZnO, dye molecules enhance photon absorption, generating electron-hole pairs that drive the photocatalytic reaction. In all cases, the PVDF-ZnO 1 wt% sample exhibits the highest degradation rate, especially during the later stages of degradation. Comparing various dyes, MO and TB demonstrate superior degradation ability compared to CR, attributed to the latter's higher structural stability. While various nanoarchitectures have been explored for photocatalytic dye degradation in the literature, this study distinguishes itself by combining nanoarchitecture with the structural stabilization of nanomaterials embedded in polymer chains to mitigate secondary pollution. This versatile approach facilitates the simple and cost-effective separation of the catalyst after photodegradation.

Table 1 presents a comparison of the experimental observations we obtained for the photocatalytic degradation efficiency with those already available in the literature. As per the table, the current system fabricated with the cheapest and least complicated method shows comparatively better results.

The efficiency of the developed catalysts in preventing secondary pollution was investigated by centrifuging the solution after photocatalysis for 6 h. Since the morphology and density of microspheres are different from that of the water medium, the particles were easily removed from the medium during centrifugation. The settled particles
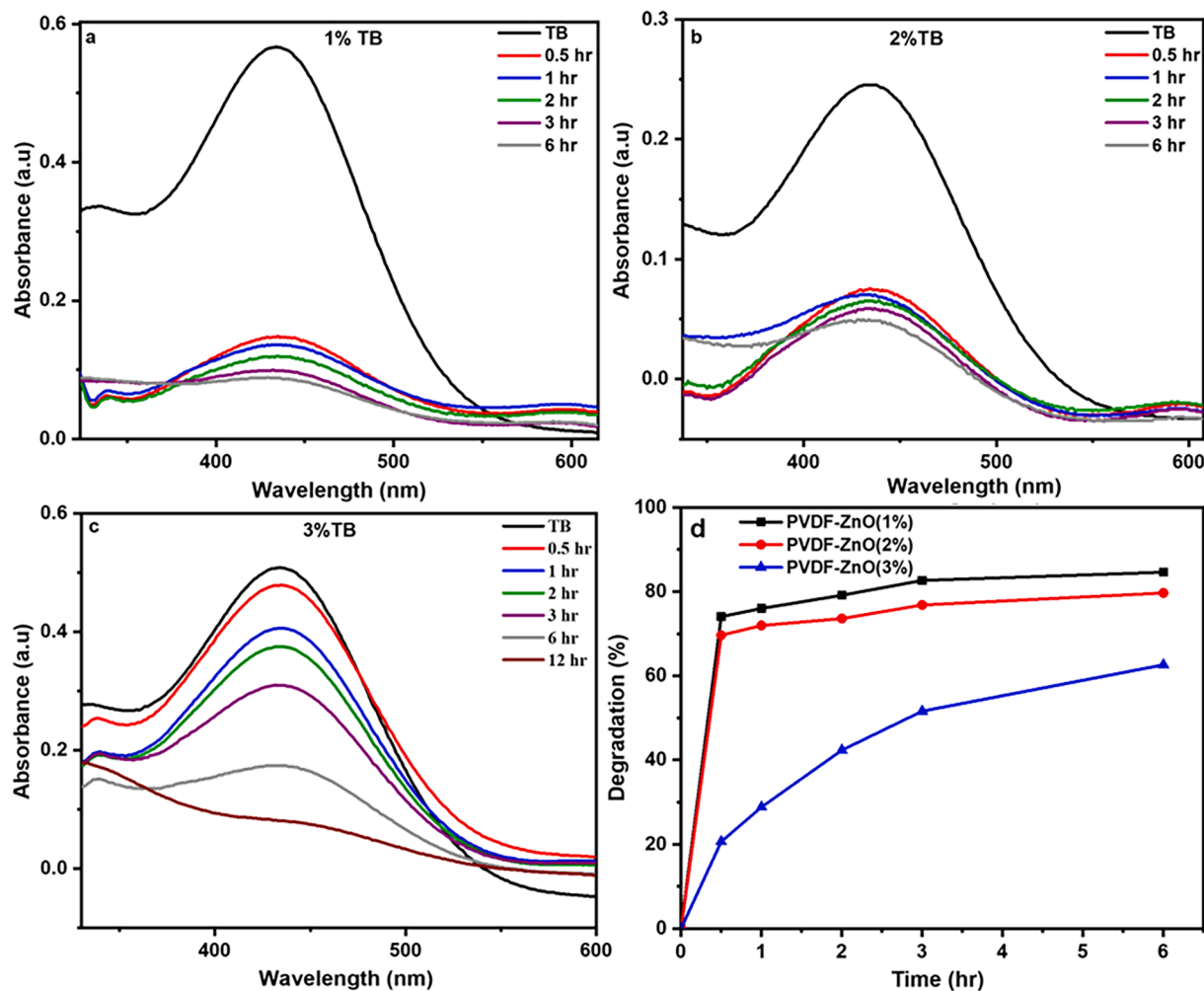
Fig. 8. The degradation of TB by PVDF-ZnO nanocomposites with different ZnO compositions a) 1 wt%, (b) 2 wt%, (c) 3 wt% and (d) comparison of degradation efficiency.
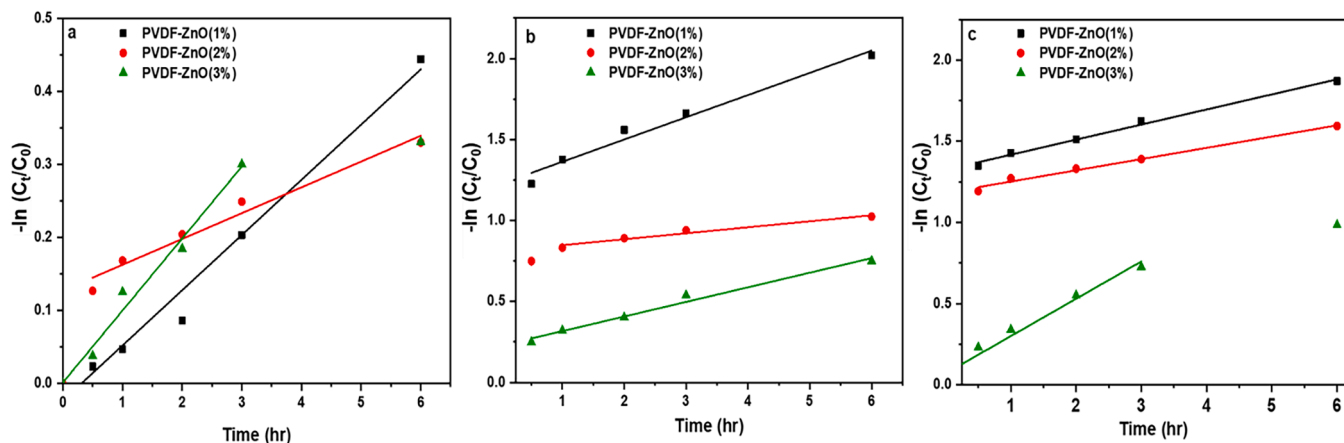

Fig. 9. Pseudo-first order rate kinetics for the degradation of (a) CR, (b) MO, and (c) TB using the PVDF-ZnO nanocomposite.

were then collected. The supernatant solution was checked for optical transparency, and the presence of particles was explored using FTIR spectral analysis, which showed no presence of polymer particles.

4. Conclusions

The PVDF-ZnO composite microspheres were prepared using a straightforward phase separation-assisted nanoprecipitation method, resulting in microspheres with excellent structural stability and crystallinity, as confirmed by XRD and FTIR spectra. The photocatalytic activity of these microspheres was evaluated by testing their ability to degrade Methyl Orange, Thymol Blue, and Cresol Red dyes under neutral pH conditions. Among the different ZnO concentrations tested in the composite, the 1 wt% ZnO composite exhibited the highest catalytic

Table 1

Comparison of current result with previously published literature.

Polymer Nanocomposite	Maximum Degradation Efficiency	Reference
CuO–ZnO nanocomposites with 20 wt% CuO	82 %	(Bekru et al., 2022)
PVDF/ZnO electrospun nanofibers with 1 wt% ZnO	85 %	(Parangusan et al., 2022)
ZnO nanoparticles	92 %	(Ekennia et al., 2021)
$Cu_7S_4/CuCo_2O_4$ yolk–shell microspheres	96.3 %	(He et al., 2023 Feb)
Z-scheme $KNbO_3/ZnIn_2S_4$ hollow core–shell microsphere	99.8 %	(He et al., 2023 Nov)
PVDF/GO/ZnO composite membranes	86.84 %	(Zhang et al., 2019 Mar)
PVDF/ ZIF-8/ZnO with 15 wt% nanomaterial	95.02 %	(Tang et al., 2022 Feb)
This work; PVDF-ZnO 1 wt%	86 %	Current Study

activity, showing great potential for practical applications. Specifically, the degradation efficiencies of PVDF-ZnO 1 wt% towards MO, TB, and CR dyes were found to be 86 %, 84 %, and 35 %, respectively, after 6 h of sunlight exposure. Moreover, these microspheres proved to be effective for degrading various types of dyes and could be easily separated from the water medium without causing secondary pollution.

CRediT authorship contribution statement

Hayarunnisa Anwar: Methodology, Formal analysis, Data curation. **Maryam Al-Ejji:** Resources, Writing – review & editing. **V. Radhika:** Visualization, Writing – original draft. **Deepalekshmi Ponnamma:** Conceptualization, Supervision, Validation, Writing – review & editing.

Declaration of competing interest

The authors declare that they have no known competing financial interests or personal relationships that could have appeared to influence the work reported in this paper.

Appendix A. Supplementary material

Supplementary data to this article can be found online at https://doi.org/10.1016/j.arabjc.2024.105670.

References

Akhtar, M.J., Alhadlaq, H.A., Alshamsan, A., Majeed Khan, M.A., Ahamed, M., 2015. Aluminum doping tunes band gap energy level as well as oxidative stress-mediated cytotoxicity of ZnO nanoparticles in MCF-7 cells. Sci. Rep. 5, 1–16.

Al-Ariki, S., Yahya, N.A.A., Al-A'nsi, S.A., Jumali, M.H.H., Jannah, A.N., Abd-Shukor, R., 2021. Synthesis and comparative study on the structural and optical properties of ZnO doped with Ni and Ag nanopowders fabricated by sol gel technique. Sci. Rep. 11, 1–11.

Baskoutas, S., Bester, G., 2010. Conventional optics from unconventional electronics in ZnO quantum dots. J. Phys. Chem. C 114, 9301–9307.

Baskoutas, S., Bester, G., 2011. Transition in the optical emission polarization of ZnO nanorods. J. Phys. Chem. C 115, 15862–15867.

Bekru, A.G., Tufa, L.T., Zelekew, O.A., Goddati, M., Lee, J., Sabir, F.K., 2022. Green Synthesis of a CuO-ZnO Nanocomposite for Efficient Photodegradation of Methylene Blue and Reduction of 4-Nitrophenol. ACS Omega 7, 30908–30919.

Devi, P.I., Ramachandran, K., 2011. Dielectric studies on hybridized PVDF-ZNO nanocomposites. J. Exp. Nanosci. 6, 281–293.

Dodd, A.C., McKinley, A.J., Saunders, M., Tsuzuki, T., 2006. Effect of particle size on the photocatalytic activity of nanoparticulate zinc oxide. J. Nanoparticle Res. 8, 43–51.

Du, C., Li, M., Cao, M., Feng, S., Guo, H., Li, B., 2018. Enhanced thermal and mechanical properties of polyvinylidene fluoride composites with magnetic oriented carbon nanotube. Carbon N Y 126, 197–207.

Ekennia, A.C., Uduagwu, D.N., Nwaji, N.N., Oje, O.O., Emma-Uba, C.O., Mgbii, S.I., et al., 2021. Green synthesis of biogenic zinc oxide nanoflower as dual agent for photodegradation of an organic dye and tyrosinase inhibitor. J. Inorg. Organomet. Polym Mater. 31, 886–897.

Fleischmann, C., Lievenbrück, M., Ritter, H., 2015. Polymers and dyes: developments and applications. Polymers (Basel) 7, 717–746.

Gonçalves, R.A., Toledo, R.P., Joshi, N., Berengue, O.M., 2021. Green synthesis and applications of zno and TIO_2 nanostructures. Molecules 26.

Gopal, P.M.S.N., 2019. Energy from Toxic Organic Waste for Heat and Power Generation, first ed. Woodhead Publishing.

Guerra, E., Llompart, M., Garcia-Jares, C., 2018. Analysis of dyes in cosmetics: challenges and recent developments. Cosmetics 5.

Handore, K., Bhavsar, S., Horne, A., Chhattise, P., Mohite, K., Ambekar, J., et al., 2014. Novel green route of synthesis of ZnO nanoparticles by using natural biodegradable polymer and its application as a catalyst for oxidation of aldehydes. J. Macromol. Sci. Part A Pure Appl. Chem. 51, 941–947.

He, Z., Xia, Y., Tang, B., Jiang, X., Su, J., 2016. Fabrication and photocatalytic property of ZnO/Cu_2O core-shell nanocomposites. Mater. Lett. 1 (184), 148–151.

He, Z., Yang, H., Su, J., Xia, Y., Fu, X., Wang, L., Kang, L., 2021. Construction of multifunctional dual Z-scheme composites with enhanced photocatalytic activities for degradation of ciprofloxacin. Fuel 15 (294), 120399.

He, Z., Yang, H., Sunarso, J., Wong, N.H., Huang, Z., Xia, Y., Wang, Y., Su, J., Wang, L., Kang, L., 2022. Novel scheme towards interfacial charge transfer between $ZnIn_2S_4$ and BiOBr for efficient photocatalytic removal of organics and chromium (VI) from water. Chemosphere 1 (303), 134973.

He, Z., Siddique, M.S., Yang, H., Xia, Y., Su, J., Tang, B., Wang, L., Kang, L., Huang, Z., 2022. Novel Z-scheme In_2S_3/Bi_2WO_6 core-shell heterojunctions with synergistic enhanced photocatalytic degradation of tetracycline hydrochloride. J. Clean. Prod. 10 (339), 130634.

He, Z., Yang, H., Wong, N.H., Ernawati, L., Sunarso, J., Huang, Z., Xia, Y., Wang, Y., Su, J., Fu, X., Wu, M., 2023. Construction of $Cu_7S_4@ CuCo_2O_4$ yolk-shell microspheres composite and elucidation of its enhanced photocatalytic activity, mechanism, and pathway for carbamazepine degradation. Small 10, 2207370.

He, Z., Fareed, H., Yang, H., Xia, Y., Su, J., Wang, L., Kang, L., Wu, M., Huang, Z., 2023. Mechanistic insight into the charge carrier separation and molecular oxygen activation of manganese doping BiOBr hollow microspheres. J. Colloid Interface Sci. 1 (629), 355–367.

He, Z., Lin, K., Wong, N.H., Sunarso, J., Xia, Y., Fu, X., Su, J., Huang, Z., Wang, Y., Tang, B., 2023. Elucidation of mechanisms, pathways, and toxicity of fabricated Z-scheme $KNbO_3/ZnIn_2S_4$ hollow core–shell composites for enhanced ciprofloxacin photodegradation. Chem. Eng. J. 1 (475), 146262.

Hezam, A., Drmosh, Q.A., Ponnamma, D., Bajiri, M.A., Qamar, M., Namratha, K., Zare, M., Nayan, M.B., Onaizi, S.A., Byrappa, K., 2022. Strategies to enhance ZnO photocatalyst's performance for water treatment: a comprehensive review. Chem. Rec. 22 (7), e202100299.

Ibrahim, R.K., Hayyan, M., AlSaadi, M.A., Hayyan, A., Ibrahim, S., 2016. Environmental application of nanotechnology: air, soil, and water. Environ. Sci. Pollut. Res. 23, 13754–13788.

Ilyas, M., Ahmad, W., Khan, H., Yousaf, S., Yasir, M., Khan, A., 2019. Environmental and health impacts of industrial wastewater effluents in Pakistan: a review. Rev. Environ. Health 34, 171–186.

Jain, R., Bhargava, M., Sharma, N., 2005. Electrochemical degradation of erythrosine in pharmaceuticals and food product industries effluent. J. Sci. Ind. Res. (India) 64, 191–197.

Kadir, E.S., Gayen, R.N., Paul, R., Biswas, S., 2020. Interfacial effects on ferroelectric and dielectric properties of GO reinforced free-standing and flexible PVDF/ZnO composite membranes: Bias dependent impedance spectroscopy. J. Alloy. Compd. 843, 155974.

Kanagaraj, J., Senthilvelan, T., Panda, R.C., Kavitha, S., 2015. Eco-friendly waste management strategies for greener environment towards sustainable development in leather industry: a comprehensive review. J. Clean. Prod. 89, 1–17.

Kang, G.D., Cao, Y.M., 2014. Application and modification of poly(vinylidene fluoride) (PVDF) membranes - A review. J Memb Sci 463, 145–165.

Khoshhesab, Z.M., Sarfaraz, M., Asadabad, M.A., 2011. Preparation of ZnO nanostructures by chemical precipitation method. Synth. React. Inorgan. Met. Nano-Metal Chem. 41, 814–819.

Li, G.Y., Di, Z.H., Guo, K., Ma, X.S., Long, Y.Z., 2020. Fabrication and piezoelectric-pyroelectric properties of electrospun PVDF/ZnO composite fibers. Mater. Res. Express 7.

Ling, Z.P., Ge, J., Stangl, R., Aberle, A.G., Mueller, T., 2013. Detailed micro raman spectroscopy analysis of doped silicon thin film layers and its feasibility for heterojunction silicon wafer solar cells. J. Mater. Sci. Chem. Eng. 01, 1–14.

Ma, X.-D., Qian, X.-F., Yin, J., Zhu, Z.-K., 2002. Preparation and characterization of polyvinyl alcohol–selenide nanocomposites at room temperature. J. Mater. Chem. 12, 663–666.

Mallakpour, S., Madani, M., 2012. Use of silane coupling agent for surface modification of zinc oxide as inorganic filler and preparation of poly(amide-imide)/zinc oxide nanocomposite containing phenylalanine moieties. Bull. Mater. Sci. 35, 333–339.

Mandeep, G.G.K., Liu, H., Shukla, P., 2019. Pulp and paper industry–based pollutants, their health hazards and environmental risks. Curr. Opin. Environ. Sci. Heal 12, 48–56.

Mishra, H.K., Gupta, V., Roy, K., Babu, A., Kumar, A., Mandal, D., 2022. Revisiting of δ−PVDF nanoparticles via phase separation with giant piezoelectric response for the realization of self-powered biomedical sensors. Nano Energy 95, 107052.

Ong, C.B., Ng, L.Y., Mohammad, A.W., 2018. A review of ZnO nanoparticles as solar photocatalysts: Synthesis, mechanisms and applications. Renew. Sustain. Energy Rev. 81, 536–551.

Parangusan, H., Ponnamma, D., Al-Maadeed, M.A., Marimuthu, A., 2018. Nanoflower-like yttrium-doped ZnO photocatalyst for the degradation of methylene blue dye. Photochem. Photobiol. 94 (2), 237–246.

Parangusan, H., Bhadra, J., Ahmad, Z., Al-Maadeed, A.S.M.A., Al-Mohannadi, A.M.A.A., Al-Thani, N., 2022. Electrospun PVDF/ZnO based composite fibers for oil absorption and photocatalytic degradation of organic dyes from waste water. Fibers Polym. 23, 1217–1224.

Patti, A., Acierno, D., 2022. Towards the sustainability of the plastic industry through biopolymers: properties and potential applications to the textiles world. Polymers (Basel) 14.

Pratihar, S., Medda, S.K., Sen, S., Devi, P.S., 2020. Tailored piezoelectric performance of self-polarized PVDF-ZnO composites by optimization of aspect ratio of ZnO nanorods. Polym. Compos. 41, 3351–3363.

Puzyn, T., Mostrag-Szlichtyng, A., 2012. Organic Pollutants Ten Years After the Stockholm Convention. IntechOpen, Rijeka.

Radwan, A.B., Mohamed, A.M.A., Abdullah, A.M., Al-Maadeed, M.A., 2016. Corrosion protection of electrospun PVDF-ZnO superhydrophobic coating. Surf. Coatings Technol. 289, 136–143.

Rajendran, S., Sivakumar, P., Babu, R.S., 2007. Studies on the salt concentration of a PVdF-PVC based polymer blend electrolyte. J. Power Sources 164, 815–821.

Rao, J.P., Geckeler, K.E., 2011. Polymer nanoparticles: Preparation techniques and size-control parameters. Prog. Polym. Sci. 36, 887–913.

Reddy, A.J., Kokila, M.K., Nagabhushana, H., Rao, J.L., Shivakumara, C., Nagabhushana, B.M., et al., 2011. Combustion synthesis, characterization and Raman studies of ZnO nanopowders. Spectrochim Acta - Part A Mol. Biomol. Spectrosc. 81, 53–58.

Singh, R., Kumar, J., Singh, R.K., Kaur, A., Sinha, R.D.P., Gupta, N.P., 2006. Low frequency ac conduction and dielectric relaxation behavior of solution grown and uniaxially stretched poly(vinylidene fluoride) films. Polymer (guildf) 47, 5919–5928.

Suresh, J., Pradheesh, G., Alexramani, V., Sundrarajan, M., Hong, S.I., 2018. Green synthesis and characterization of zinc oxide nanoparticle using insulin plant (Costus pictus D. Don) and investigation of its antimicrobial as well as anticancer activities. Adv. Nat. Sci. Nanosci. Nanotechnol. 9.

Suwanboon, S., Amornpitoksuk, P., 2012. Preparation of Mg-doped ZnO nanoparticles by mechanical milling and their optical properties. Procedia Eng. 32, 821–826.

Talam, S., Karumuri, S.R., Gunnam, N., 2012. Synthesis, characterization, and spectroscopic properties of ZnO nanoparticles. ISRN Nanotechnol. 2012, 1–6.

Tang, T., Li, C., He, W., Hong, W., Zhu, H., Liu, G., Yu, Y., Lei, C., 2022. Preparation of MOF-derived C-ZnO/PVDF composites membrane for the degradation of methylene blue under UV-light irradiation. J. Alloy. Compd. 15 (894), 162559.

Tsai, M.H., Huang, Y.C., Tseng, I.H., Yu, H.P., Lin, Y.K., Huang, S.L., 2011. Thermal and mechanical properties of polyimide/nano-silica hybrid films. Thin Solid Films 519, 5238–5242.

Wooten, A.J., Werder, D.J., Williams, D.J., Casson, J.L., Hollingsworth, J.A., 2009. Solution-liquid-solid growth of ternary Cu-In-Se semiconductor nanowires from multiple- and single-source precursors. J. Am. Chem. Soc. 131, 16177–16188.

Yang, K., Huang, X., Fang, L., He, J., Jiang, P., 2014. Fluoro-polymer functionalized graphene for flexible ferroelectric polymer-based high-k nanocomposites with suppressed dielectric loss and low percolation threshold. Nanoscale 6, 14740–14753.

Zhang, D., Dai, F., Zhang, P., An, Z., Zhao, Y., Chen, L., 2019. The photodegradation of methylene blue in water with PVDF/GO/ZnO composite membrane. Mater. Sci. Eng. C 1 (96), 684–692.

Zhang, Q., Dandeneau, C.S., Zhou, X., Cao, C., 2009. ZnO nanostructures for dye-sensitized solar cells. Adv. Mater. 21, 4087–4108.

Zhao, K., Shen, A., 2012. Increasing ZnO growth rate by modifying oxygen plasma conditions in plasma-assisted molecular beam epitaxy. World J. Condens. Matter Phys. 02, 160–164.

Zhou, J., Zhao, F., Wang, Y., Zhang, Y., Yang, L., 2007. Size-controlled synthesis of ZnO nanoparticles and their photoluminescence properties. J. Lumin. 122–123, 195–197.